

Provided for non-commercial research and education use.
Not for reproduction, distribution or commercial use.



(This is a sample cover image for this issue. The actual cover is not yet available at this time.)

This article appeared in a journal published by Elsevier. The attached copy is furnished to the author for internal non-commercial research and education use, including for instruction at the authors institution and sharing with colleagues.

Other uses, including reproduction and distribution, or selling or licensing copies, or posting to personal, institutional or third party websites are prohibited.

In most cases authors are permitted to post their version of the article (e.g. in Word or Tex form) to their personal website or institutional repository. Authors requiring further information regarding Elsevier's archiving and manuscript policies are encouraged to visit:

<http://www.elsevier.com/copyright>



Contents lists available at SciVerse ScienceDirect

Earth and Planetary Science Letters

journal homepage: www.elsevier.com/locate/epsl

Displaced helium and carbon in the Hawaiian plume

Albrecht W. Hofmann^{a,b,*}, Cinzia G. Farnetani^c, Marc Spiegelman^a, Cornelia Class^a^a Lamont Doherty Earth Observatory, Palisades, NY 10964, USA^b Max-Planck-Institut für Chemie, Postfach 3060, 55020 Mainz, Germany^c Institut de Physique du Globe de Paris, Sorbonne Paris Cité, Univ Paris Diderot, UMR 7154, 75005 Paris, France

ARTICLE INFO

Article history:

Received 5 April 2011

Received in revised form 15 September 2011

Accepted 25 September 2011

Available online xxx

Editor: Y. Ricard

Keywords:

mantle plumes

Hawaii

helium

carbonatite melt

metasomatism

ABSTRACT

High relative abundances of primordial ^3He are commonly found in ocean island basalts (OIB) thought to be derived from mantle plumes, and high $^3\text{He}/^4\text{He}$ ratios have been used to distinguish plume-type from non-plume OIBs. In simple plume models, one expects to find the highest $^3\text{He}/^4\text{He}$ ratios in the axial part of the plume conduit, which is sampled during the shield building stage of the volcanoes. However, the actual locus of the highest $^3\text{He}/^4\text{He}$ ratios is sometimes significantly displaced. This is best documented for the Hawaiian plume, where the highest- $^3\text{He}/^4\text{He}$ basalts are found on Loihi, a volcano tens of kilometers ahead of the inferred plume center, and $^3\text{He}/^4\text{He}$ ratios decrease systematically toward MORB-type values during the main and late phases of eruption. We propose that this effect is caused by small amounts of carbonatite melt formed in plumes as they rise through the transition zone. If the plume conduit is tilted by plate-driven upper mantle flow, the carbonatite melt infiltrates more vertically due to its low density and viscosity and is thus displaced from the plume center. Helium, if partitioned into the carbonatite melt, will also be displaced from the plume center. To test this model we use a numerical simulation of the Hawaiian plume interacting with the fast-moving Pacific lithosphere. We obtain vertical separation velocities of the carbonatite melt on the order of a meter/year. Consequently, helium and carbon, initially located in the plume center at >450 km depth, are laterally displaced by 50 to 80 km in the shallow mantle, depending on grain size, porosity and melt production rate. This can explain why the highest $^3\text{He}/^4\text{He}$ ratios (R/R_a up to 39; $R/R_a \equiv (^3\text{He}/^4\text{He})_{\text{sample}} / (^3\text{He}/^4\text{He})_{\text{atmosphere}}$) occur on pre-shield Loihi, why they decline during the shield phases of Mauna Loa, Mauna Kea and Haleakala, and why post-shield and rejuvenated Hawaiian volcanism delivers only low $^3\text{He}/^4\text{He}$ ratios ($R/R_a = 8-10$). Our results quantify the potential role of carbonatite liquids in transporting helium in the Hawaiian conduit, and they appear to apply also to other plumes tilted by upper-mantle 'wind'.

© 2011 Elsevier B.V. All rights reserved.

1. Introduction

The survival of primordial helium-3 in the Earth's mantle has led many authors to use helium isotopes to constrain models of mantle dynamics and evolution. One first-order interpretation is that primordial helium (identified by its high $^3\text{He}/^4\text{He}$ ratio) is located in a deep-mantle reservoir (Allègre and Moreira, 2004; Courtillot et al., 2003; Farley et al., 1992; Graham, 2002; Kurz et al., 1983; Samuel and Farnetani, 2003; Tolstikhin and Hofmann, 2005) or in incompletely degassed portions of a depleted lower mantle (Class and Goldstein, 2005; Gonnemann and Mukhopadhyay, 2009) and can be used to trace convective plumes derived from the lower mantle. Examples of such high- $^3\text{He}/^4\text{He}$ hotspots are Hawaii, Iceland, Samoa, Galápagos, Juan Fernandez, Pitcairn, Society Islands, Azores, Yellowstone, Afar, and Kola

Peninsula. Thus, while the debate about the location of source reservoir(s) of this primordial ^3He continues, here we rely on recent versions of Earth models invoking deep-mantle plumes as carriers of primordial helium. Tolstikhin and Hofmann (2005) and Tolstikhin et al. (2006) have proposed a model in which the so-called D" layer, identified by seismology and located at the base of the mantle, serves as reservoir of primordial helium brought to the surface by mantle plumes. This model has received independent support by evidence based on meteoritic and terrestrial ^{142}Nd abundances, favoring the existence of an ancient hidden reservoir, created shortly after the accretion of the Earth (Boyet and Carlson, 2005). We will use the scenario in which deep mantle plumes rise from a boundary layer near the core-mantle boundary as our starting point. We further assume that the highest $^3\text{He}/^4\text{He}$ ratios are initially concentrated in the core of the rising plumes (e.g. Kurz et al., 1996), because the high- $^3\text{He}/^4\text{He}$ enters the plume source from below, e.g. from the D" layer (Samuel and Farnetani, 2003; Tolstikhin and Hofmann, 2005) or conceivably from the core (Porcelli and Halliday, 2001).

Although the geographic association of high- $^3\text{He}/^4\text{He}$ basalts with inferred mantle plumes is strong, detailed regional studies have revealed several instances where the high- $^3\text{He}/^4\text{He}$ signal is locally

* Corresponding author at: Lamont Doherty Earth Observatory, Palisades, NY 10964, USA.

E-mail addresses: albrecht.hofmann@mpic.de (A.W. Hofmann), cinzia@ipgp.fr (C.G. Farnetani), mstieg@ldeo.columbia.edu (M. Spiegelman), class@ldeo.columbia.edu (C. Class).

displaced from the inferred plume center and, possibly, also decoupled from other tracers of mantle plumes, such as Sr, Nd, and Pb isotopes. Such displacements are seen most prominently on Hawaiian volcanoes (DePaolo et al., 2001; Hanyu et al., 2005; Kurz et al., 1996; Valbracht et al., 1996) but also on the Galápagos Islands (Harpp and White, 2001), the Reykjanes Ridge (Breddam et al., 2000; Taylor et al., 1997) and on the SEIR near Amsterdam (Graham et al., 1999). What mechanism might cause such displacements? Because of helium's volatile nature, several authors have suggested a shallow-mantle metasomatic process, involving either aqueous or CO₂-rich fluids (Kurz et al., 1996; Valbracht et al., 1996), volatile-rich silicate melt movement (DePaolo et al., 2001) or, most recently, carbonatite liquids (Dixon et al., 2008). However, all these mechanisms require a significant lateral component in the direction of metasomatic movement (most clearly seen in the cartoons of Dixon and Clague, 2001; Hanyu et al., 2005; Valbracht et al., 1996), in order to explain the observed lateral displacement of the helium signal. This is troublesome, because there is no obvious horizontally directed driving force for such fluid movement. In this paper, we address this problem in a somewhat different way: While building on the previous ideas, we develop scenarios whereby it is the plume that moves laterally, whereas the metasomatic fluid migrates vertically, driven only by gravity. Our three dimensional numerical simulations of the Hawaiian plume (Farnetani and Hofmann, 2010) showed that the conduit in the upper mantle is tilted in the direction of the Pacific plate motion. Here we use the temperature and velocity fields of this Hawaiian plume model to calculate the onset of carbonate melting and the subsequent flow of the carbonatite liquids within the conduit.

Before developing our model quantitatively, we briefly review the evidence of asymmetric, lateral displacements of the helium signal from the plume center and for the separation (decoupling) of ³He/⁴He from other isotopic plume tracers. We then summarize the evidence for deep carbonate melting in the upper mantle, for helium partitioning relative to other trace elements, for elevated carbon contents in mantle plumes, and finally the theory of migration rates of carbonatite liquids in rising mantle plumes. The combination of these elements enables us to model the expected distribution of R/Ra (where $R/Ra \equiv (^3\text{He}/^4\text{He})_{\text{sample}} / (^3\text{He}/^4\text{He})_{\text{atmosphere}}$; with $Ra = 1.4 \times 10^{-6}$) at sublithospheric depth and its sampling by the Hawaiian volcanoes. We show that high values of R/Ra in the pre-shield stage, followed by declining values during the shield and post-shield stages, are obtained if the carbonatite liquids, not the solid silicate plume material, carry the high R/Ra values.

2. Evidence for lateral helium displacement and 'decoupling' in mantle plumes

The asymmetric distribution of ³He/⁴He in the evolution of Hawaiian volcanoes was noted by Kurz and Kammer (1991), Kurz et al. (1995), Kurz et al. (1996) and Valbracht et al. (1996). As a rule, ³He/⁴He ratios of Hawaiian volcanoes start with high values during the early phases of growth, then decline during the main shield-building stage, and reach low, MORB-like values during late, post-shield and the even later, 'rejuvenated', stages of volcanism. During its initial, pre-shield, phase of alkalic volcanism, each Hawaiian volcano samples the leading edge of the plume's melting region located well ahead of the plume center (Farnetani and Hofmann, 2010), and delivers lavas with high ³He/⁴He ratios (R/Ra up to 39 in the case of Loihi). Because these pre-shield lavas are later covered by voluminous, shield-stage lavas, the only volcano that has been sampled extensively in its pre-shield-stage is Loihi (see Fig. 1 for a map of Hawaiian volcanoes). There are only two other locations where clearly pre-shield, alkaline lavas have been sampled, the South Arch volcanic field, located about 200 km south of Hawaii, and the submarine Hilina section on the eastern flank of Kilauea Volcano. It is thought to contain primarily pre-shield Kilauea basalts, but some of the lavas sampled in this region may be derived from Loihi and Mauna Loa

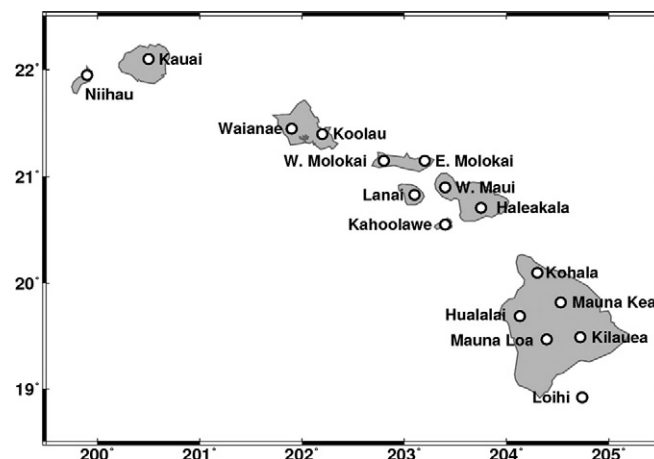


Fig. 1. Map of Hawaiian volcanoes.

(Hanyu et al., 2010). Fig. 2 shows helium data for these three pre-shield suites and juxtaposes them with late-stage, also predominantly alkalic lavas (and some xenoliths carried by them) from so called post-shield and/or rejuvenated stages of seven other Hawaiian volcanoes (Mauna Kea, Hualalai, Haleakala, Molokai, Koolau, Niihau and Kauai). Although the ³He/⁴He ratios of the Hilina and South Arch basalts are not as

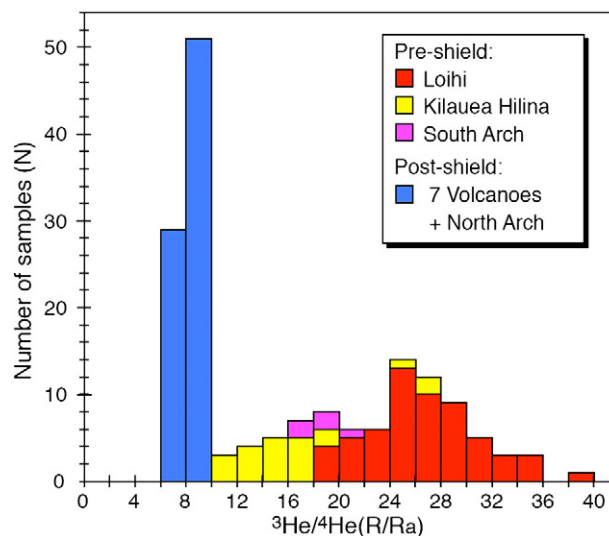


Fig. 2. R/Ra values ($R/Ra \equiv (^3\text{He}/^4\text{He})_{\text{sample}} / (^3\text{He}/^4\text{He})_{\text{atmosphere}}$) in pre-shield versus post-shield Hawaiian lavas illustrate the fundamental asymmetry of helium isotope distribution between early and late phases of eruptive history. Pre-shield lavas are for (1) Loihi alkali basalts and tholeiites, (2) submarine lavas from the Hilina region representing primarily pre-shield Kilauea, but possibly including lavas derived from Loihi and Mauna Loa, and (3) alkali basalts from the South Arch. The latter are not strictly speaking derived from a 'pre-shield' volcano but have compositions clearly related to the plume and are located on the upstream edge of the Hawaiian topographic swell. Post-shield samples are for alkaline lavas and xenoliths from seven Hawaiian volcanoes in their post-shield or rejuvenated phases. Volcanoes included are Mauna Kea (post shield lavas), Hualalai (post-shield lavas and xenoliths), Haleakala (post-shield lavas), Molokai (rejuvenated basalts), Koolau (rejuvenated basalts and xenoliths), Kauai (rejuvenated basalts), Niihau (rejuvenated basalts). Basalts from the North Arch are consistent with post-shield and rejuvenated phases. All the post-shield data fall in the narrow range of $6.2 < R/Ra < 9.8$ and are thus indistinguishable from ordinary MORB. Data from: Allègre et al. (1983), Althaus et al. (2003), Craig and Poreda (1986), Garcia et al. (1998), Hanyu et al. (2005), Hanyu et al. (2010), Honda et al. (1991), Honda et al. (1993), Hyagon et al. (1992), Kaneoka et al. (1983), Kent et al. (1999), Kurz (1986), Kurz et al. (1983), Kurz et al. (2004), Kyser and Rison (1982), Matsumoto et al. (2008), Mukhopadhyay et al. (2003), Porcelli et al. (1987), Ren et al. (2009), Rison and Craig (1983), Sarda et al. (1988), Staudacher et al. (1986), Trull et al. (1993), Valbracht et al. (1996), Valbracht et al. (1997), and Vance et al. (1989).

high as the more extreme Loihi samples, they are nevertheless consistently higher than the He ratios of any of the late-stage lavas or xenoliths, all of which have $^3\text{He}/^4\text{He}$ ratios indistinguishable from MORB values ($7 < R/Ra < 10$).

During the shield-building stage, the volcanoes issue tholeiitic lavas that sample melting regions close to the plume center. The only three Hawaiian volcanoes for which long-term records of this shield stage are available, Mauna Loa, Mauna Kea and Haleakala, all show consistently declining $^3\text{He}/^4\text{He}$ ratios as each volcano ages (Fig. 3, see figure caption for references). Thus the 200 ka record for Mauna Loa, and the 600 ka record for Mauna Kea, (Fig. 3a) yield R/Ra values that decline from 15 to 20 for the oldest lavas to MORB-like values of 8 to 10 at the later stages of evolution, as each volcano moves from a relatively central position above the plume melting region toward the trailing edge. The less continuous but nevertheless long-term record of Haleakala shows similarly declining R/Ra values (Fig. 3b).

Blichert-Toft and Albarède (2009) have argued that some of the lavas sampled by the deeper parts of the HSDP drill core on Mauna Kea (i.e. those labeled 'hi-8' basalts by Eisele et al., 2003) are geochemically distinct from other Mauna Kea lavas and might not originate from Mauna Kea at all, but from another, 'lost' volcano. Nevertheless, Fig. 3a shows that, even if the samples assigned to this 'lost' volcano (identified by Pb isotopes marked in yellow) are

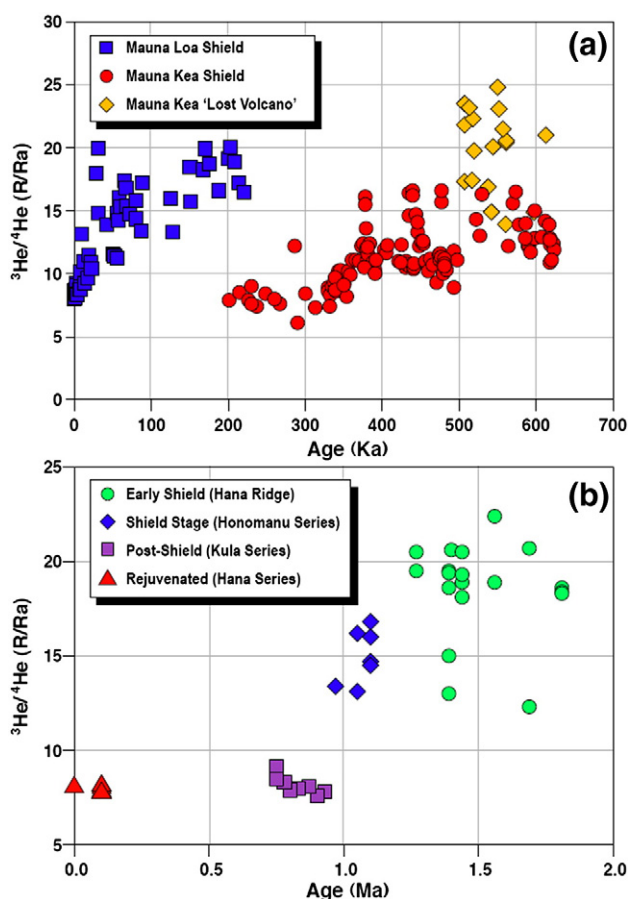


Fig. 3. (a) R/Ra versus eruption age for shield stages of Mauna Loa and Mauna Kea. Similar plots for these two volcanoes have been shown by Kurz et al. (2004). In both volcanoes, R/Ra values decline as the volcano ages (i.e., for younger eruption age). Mauna Loa is currently in a late shield stage, Mauna Kea in a post-shield stage. Data from: Althaus et al. (2003), Kurz and Kammer (1991), Kurz et al. (1987), Kurz et al. (1995), and Kurz et al. (2004). (b) R/Ra versus eruption age for Haleakala Volcano (Maui) covering shield, post-shield, and rejuvenated phases. The ages of the post-shield Kula Series lavas have been interpolated between ages measured on different samples in the same drill core. Data from: Craig and Poreda (1986), Hanyu et al. (2007), Kurz (1986), Kurz et al. (1987), Marti and Craig (1987), and Scarsi (2000).

excluded from consideration, the age-controlled, long-term decline of $^3\text{He}/^4\text{He}$ on Mauna Kea still holds true.

A possible exception to the above general pattern exists on the island of Kauai: moderately high $^3\text{He}/^4\text{He}$ values ($17 < R/Ra < 28$) occur in lavas erupted late in its shield-building phase (Mukhopadhyay et al., 2003), and this contrasts with the decline of $^3\text{He}/^4\text{He}$ values observed on other Hawaiian volcanoes at this stage of their evolution. However, the geological and temporal relationships on Kauai are uncertain; for example it is not clear whether Kauai represents a single volcano or two separate volcanoes (Mukhopadhyay et al., 2003). Thus, long-term stratigraphically controlled data are needed to establish whether Kauai does represent a true exception to an otherwise general Hawaiian pattern of declining $^3\text{He}/^4\text{He}$ ratios as a given volcano ages.

The overall evidence reviewed above demonstrates a common pattern of high $^3\text{He}/^4\text{He}$ ratios during the incipient stages of Hawaiian volcanism, followed by lower and generally declining $^3\text{He}/^4\text{He}$ during the main shield-building stages, and low, MORB-like values during the final stages. This suggests that helium with the highest R/Ra has been displaced from the hottest, central part of the plume sampled by tholeiitic magmas toward the plume's 'leading edge' sampled by alkalic magmas. Likewise, MORB-like helium originating from outside the plume appears to have invaded the trailing edge of the plume sampled by post-shield and rejuvenated magmas.

There are several other cases where high- $^3\text{He}/^4\text{He}$ signatures in basalts are evidently displaced. These include ridge basalts in the vicinity of the Amsterdam-St. Paul plume (Nicolaysen et al., 2007), and OIBs from one of the Galápagos Islands, Fernandina (Graham, 2002). Here we illustrate one example for the Iceland plume. Fig. 4 shows $^3\text{He}/^4\text{He}$ and $^{87}\text{Sr}/^{86}\text{Sr}$ ratios, plotted as a function of latitude, in basalts from Iceland and the adjacent regions of the mid-Atlantic Ridge to the north and the south. $^{87}\text{Sr}/^{86}\text{Sr}$ ratios on the Reykjanes Ridge decline southward to typical, depleted-MORB values of 0.7027 at about 61°N. At this same latitude, $^3\text{He}/^4\text{He}$ remains uniformly high at around R/Ra ~ 15, for more than another 200 km, to about 59°N. Hilton et al. (2000) have shown that the helium versus lead isotope ratios along the Reykjanes Ridge can in principle be explained by binary mixing between plume and MORB-mantle, as a possible consequence of a preferred southward flow of plume material along the ridge at shallow, sublithospheric depths. On the other hand, at greater depth, the global upper mantle flow is northward, according to the mantle circulation model of Mihalffy et al. (2008), which is based on shear-wave splitting and tomography-derived relative mantle densities. In addition, there is evidence from receiver function seismology (Shen et al., 2002) that the Iceland plume is tilted toward the north, because the minimum thickness of the transition zone, tracing the hottest part of the plume, is displaced to the south by at least 100 km. Thus, it seems likely that the Icelandic plume conduit is tilted, and that at least part of its helium signal is displaced toward the 'upwind' side of the tilted plume.

A separate question is whether the helium signal, in addition to being displaced from the plume center, may also be 'decoupled' from other isotope tracers, particularly Sr, Nd, Hf, and Pb, in the sense that the He signal is displaced by a greater distance from the plume core than the other tracers. The asymmetry and displacement of He signals from the Hawaiian plume center has led some authors to postulate such 'decoupling'. Valbracht et al. (1996) first suggested a separation mechanism by rising, volatile-rich, incipient melts, which then metasomatize the lithosphere. A similar decoupling has been suggested by DePaolo et al. (2001), who constructed contour maps of different isotopic tracers for Loihi and the Island of Hawaii: Most of these tracers of the plume, e.g. the lowest $^{143}\text{Nd}/^{144}\text{Nd}$ ratios, are centered near Mauna Loa and Kilauea, close to the present-day plume center, where the most voluminous magma production is taking place. In contrast, the highest R/Ra values are centered around Loihi. Decoupling of helium from lithophile tracers of Hawaiian

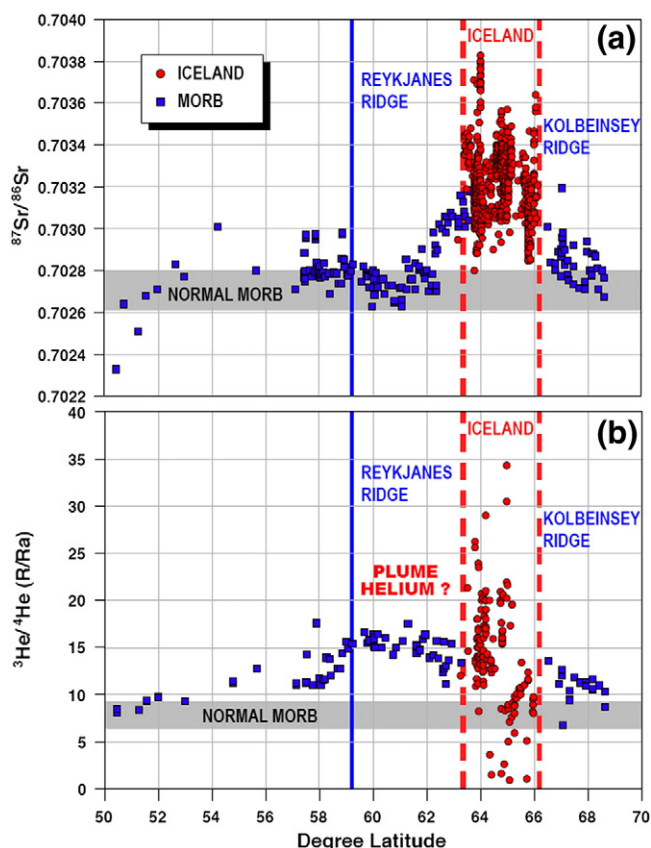


Fig. 4. (a) Sr and (b) He isotopes versus latitude across Iceland, the Reykjanes Ridge (to the south) and the Kolbeinsey Ridge (to the north). In contrast to the roughly symmetrical distribution of Sr isotopes on the ridge segments, helium isotopes are distinctly skewed toward high R/Ra values on the Reykjanes Ridge. Data from: Brandon et al. (2007), Breddam et al. (2000), Condomines et al. (1983), Dixon (2003), Dixon et al. (2000), Hilton et al. (2000), Jackson et al. (2008), Kurz et al. (1985), Licciardi et al. (2006), Macpherson et al. (2005), Moreira et al. (2001), Murton et al. (2002), Poreda et al. (1986), Schilling et al. (1999), and Taylor et al. (1997).

plume components by carbonatite metasomatism, especially around the plume margin, has also been invoked by Dixon et al. (2008).

Nevertheless, the reality of decoupling of He from Sr, Nd, Hf, and Pb isotopes on Hawaiian volcanoes remains controversial. Thus, Eiler et al. (1998), using a three-component principal component analysis (PCA), showed that He and Pb isotopes for Hawaiian pre-shield and shield lavas are strongly correlated. Mukhopadhyay et al. (2003), using a four-component PCA including Sr and Nd, in addition to Pb isotopes, produced an even better fit for 60 Hawaiian pre-shield and shield lavas. Finally, Hanyu et al. (2010) reaffirmed that He isotopes are strongly coupled to lithophile radiogenic isotopes in pre-shield Kilauea lavas. However, none of the datasets used in these efforts included post-shield or rejuvenated Hawaiian lavas. Moreover Dixon et al. (2008) have emphasized that pre-shield and rejuvenated Hawaiian magmas are very similar except for their helium isotopic compositions. Thus, it may well be that He and lithophile isotope systems are coupled during the pre-shield and shield phases, but become decoupled during the post-shield and rejuvenated stages of Hawaiian volcanism. For the present purpose, the question of decoupling is interesting but somewhat secondary to the much more clear-cut evidence for displacement of the high-He signal from the center of the plume toward its leading edge.

3. Deep carbonate melting and helium partitioning

Earlier experimental work on carbonate melts had concentrated on elucidating the origin of carbonatite magmas and included

numerous experimental studies for well over thirty years (Koster van Groos and Wyllie, 1973; Lee and Wyllie, 1996). Because of experimental limitations, most of these studies were limited to pressures corresponding to less than 100 km depth. However, mantle xenoliths and micro-inclusions in diamonds suggest that carbonatite liquids or carbonate-rich kimberlite melts can form at much deeper levels in the Earth's mantle. More recent experiments extended the range of pressures to about 9 GPa (Dasgupta and Hirschmann, 2006), and up to 20 GPa (Ghosh et al., 2007, 2009), showing that carbonate liquids can form throughout much of the upper mantle even at very low CO_2 abundances of 100 to 1000 ppm (Dasgupta et al., 2004; Hammouda, 2003; Yaxley and Brey, 2004). Dasgupta and Hirschmann (2006) inferred the lower limit of existence of such liquids to be at 300 km beneath ridges and about 400 km within hotter mantle plumes, although the stability of such liquids depends strongly on the local oxygen fugacity (Stagno and Frost, 2010). Hirschmann (2010) parameterized published experimental melting data on carbonated hydrous peridotite. He showed that the carbonatite melts formed in the deeper part of the upper mantle are replaced by hydrous silicate melts at shallower levels, and noted that "there is probably a continuum between true carbonatites and carbonated silicate melts, particularly at pressures above 3 GPa."

Minarik and Watson (1995) demonstrated a very high permeability of peridotite in the presence of carbonate liquid, and Hammouda and Laporte (2000) showed experimentally that carbonate liquids can percolate through mantle rock at remarkably high rates of up to 1 m/yr. Both of these studies therefore confirm the potential power of carbonatite liquids for causing large-scale metasomatic transport in the mantle.

Dasgupta and Hirschmann (2006) pointed out that carbonatite liquids could be important carriers of mantle helium. In order for such a mechanism to separate helium from other isotope tracers such as Sr, Nd, Hf, and Pb, solid-melt partition coefficients of these elements must be different from helium partitioning. The most recent experimental results for partitioning between mantle minerals and carbonate melts show that the partition coefficients of most incompatible trace elements are remarkably similar for carbonate and silicate liquids, except for a few elements like Ti, Zr, and Hf, which have significantly higher partition coefficients in the presence of carbonatite melt (Dasgupta et al., 2009).

For helium, some recent experimental determinations yielded partition coefficients $D(\text{He}) \sim 10^{-4}$ for both olivine and clinopyroxene (Heber et al., 2007), whereas others obtained values of $D(\text{He}) = 2$ to 5×10^{-3} for olivine, closer to, but still lower than, the coefficients for Sr, Nd, Pb and Hf (Parman et al., 2005). Heber et al. (2007) argued that submicroscopic gas bubbles not eliminated in Parman's experiments might account for the difference, so that the lower value should be closer to the correct value. Burnard et al. (2010) determined solubilities of He and Ar in carbonatite liquids at atmospheric pressure and found that they are similar to the respective solubilities in silicate liquids. Overall, the experimental issues are far from settled.

If the estimate of $D(\text{He}) \leq 10^{-4}$ is correct, the scenario invoked by Dasgupta et al. (2009), involving a mantle carbon content of 300 ppm, will cause the carbonatite melt to sequester essentially all of the helium, while leaving about 90% of the Nd and Pb, and more than 95% of the Sr in the solid phases. If such a carbonatite moves upward sufficiently rapidly, and the plume is tilted by a horizontal component of upper-mantle flow, this will begin to separate the helium from Sr, Nd, Hf, and Pb. On the other hand, if $D(\text{He})$ is as high as 10^{-3} or 10^{-2} , the helium may remain more closely coupled to Sr, Nd, Hf, and Pb, as suggested by Mukhopadhyay et al. (2003).

4. Carbon content of the upper mantle and of plumes

The knowledge of the carbon concentration is necessary to estimate the migration rates of carbonatite liquids in a rising plume,

and to assess the partitioning of He and other trace elements into carbonatite liquids formed at high pressures. However, the carbon concentration is difficult to estimate because carbon is nearly always degassed from lavas during or before eruption. In MORB, this problem can sometimes be circumvented because lavas erupted at sufficient depth occasionally do retain their volatile budget. Thus, Saal et al. (2002) have shown remarkable correlations between CO₂ and Nb (CO₂/Nb = 239) in extremely depleted, vapor-undersaturated, and therefore undegassed MORB from the Sequeiros Fracture Zone in the Pacific Ocean, and they estimated the CO₂ concentration of the depleted ('N-MORB') mantle at 72 ± 19 ppm. Subsequently, Cartigny et al. (2008) showed that 'popping rocks' from 14°N on the mid-Atlantic Ridge have higher CO₂/Nb ratios of about 540 and are positively correlated with La/Sm, indicating that CO₂/Nb ratios in MORB sources are heterogeneous and reflect the degree of previous depletion or enrichment. Cartigny et al. (2008) inferred an average CO₂ content of 1800 ppm for average MORB, corresponding to about 180 ppm CO₂ in MORB source mantle, in reasonable agreement with the earlier estimate of about 140 ppm by Marty and Tolstikhin (1998), based on C/³He ratios in MORB.

Mantle plumes, and OIB sources in general, are almost always enriched in incompatible elements relative to MORB sources, so that their carbon contents are almost certainly significantly greater than 180 ppm. Unfortunately, direct measurements of CO₂ are not useful guides to the CO₂ contents of primary OIB magmas, because no carbon-undersaturated samples have been found that would be suitable for such measurements. Essentially all Hawaiian basalts have lost CO₂ prior to eruption, so CO₂ contents of lavas cannot be used to infer the carbon content of mantle source (Dixon and Clague, 2001). One way around this problem is to apply the MORB-derived CO₂/Nb ratio of 530 of Cartigny et al. (2008) to obtain a minimum estimate for the CO₂ content of the plume from the Nb concentration of the plume basalt. Thus, and in combination with estimates for a primary Nb content (6.5 ppm) and an effective enrichment factor of nine over the bulk source composition, given by Sobolev et al. (2005) for Mauna Loa lavas, we obtain a CO₂ content of 380 ppm for the Mauna Loa source. As noted, this is a minimum estimate because CO₂/Nb ratios correlate positively with incompatible-element enrichment of mantle rocks (Cartigny et al., 2008), so that the Hawaiian source is actually expected to have a CO₂/Nb ratio greater than 530. Independent estimates of the primary CO₂ content of Hawaiian lavas have been made by Dixon and Clague (2001) and by Gerlach and Graeber (1985) on the basis of the maximum vesicularity found in these lavas, which is almost entirely ascribed to CO₂ degassed from the melt. Maximum vesicularities of Loihi and Kilauea lavas translate into CO₂ contents of 0.65 and 0.63 wt.%, or 6500 ppm CO₂ respectively. This, using the same melt/source enrichment factor of nine given by Sobolev et al. (2005), leads to a CO₂ content of 720 ppm for the Mauna Loa source. For the purpose of this paper we will use a range of 380 to 720 ppm CO₂ in the plume, which upon melting translates to 870 and 1650 ppm CaCO₃ carbonate melt in the plume. In the following section, we will use these amounts as melt fractions of carbonatite melt to calculate the melt ascent velocities within the plume.

5. Migration of carbonatite liquids in the plume

The potential efficiency of carbonatite liquids as agents of large-scale metasomatism in the mantle rests on the unique physical properties of such liquids: their low density, low viscosity, and high permeability of the peridotite matrix. Density and viscosity have been determined experimentally, with values of about 2200 kg m⁻³ and 5 × 10⁻³ Pa s, respectively (Treiman and Schedl, 1983). The permeability of the peridotite matrix depends strongly on the connectivity of the melt in a three-dimensional network of grain boundaries or grain-corner channels. Using diffusion experiments to determine

the lower limit of carbonatite melt connectivity in an olivine matrix, Minarik and Watson (1995) found that such melts are connected through channels along grain corners down to porosities of 5 × 10⁻⁴. The permeability of a mantle rock to an interconnected liquid is

$$k = \frac{d^2 \phi^n}{C} \quad (1)$$

where d is the grain diameter, ϕ the porosity, with the exponent estimated at $n=3$ and the geometric parameter estimated at $C=270$ (Wark et al., 2003). Recent modeling experiments that use a centrifuge apparatus to drive the segregation of a silicate melt from a peridotite matrix at high pressure (0.9 to 1.4 GPa) suggest higher permeabilities and much lower values of $C=3$ to 27 (Connolly et al., 2009). However, the models do not include the large centrifugal acceleration across the sample. In the following derivation of the relevant transport equations, we assume that there is no threshold porosity, because it seems likely that the lower limit of connectivity determined by Minarik and Watson (1995) may not directly apply to a material undergoing shear deformation during the infiltration process.

Given the expected mobility of carbonatite melts we can use some simplified magma-dynamics theory to make estimates of the distribution of carbonatite melts and transport paths through the mantle. In the absence of viscous compaction effects and small porosities, the equations of melt transport can be described using the "zero compaction length approximation" (Spiegelman, 1993a, 1993b) which says that the evolution of porosity in a 3-D melting and solid flow field can be described by the evolution equation

$$\frac{\partial \phi}{\partial t} + \mathbf{u}_\phi \cdot \nabla \phi = \frac{\Gamma}{\rho_l} \quad (2)$$

where

$$\mathbf{u}_\phi = \mathbf{U}_s + \frac{\partial k}{\partial \phi} \frac{\Delta \rho g}{\mu} \mathbf{k} \quad (3)$$

is the velocity field along which porosity propagates and Γ is the rate of mass transfer from solid to liquid (i.e. melting rate). \mathbf{U}_s is the solid velocity field, k the permeability (Eq. (1)), $\Delta \rho = \rho_l - \rho_s$ is the density difference between melt and solid, g gravity, and μ fluid viscosity.

If the melting rate Γ is known, Eq. (2) can be solved by the method of characteristics to estimate the porosity field and the direction of transport. In particular, for regions where there is no mass transfer ($\Gamma=0$), porosity remains constant along characteristics and will be set by the porosity at the end of carbonatite melting (see below). The important feature of Eq. (3) is that the transport velocity (as well as the trajectories of any trace element; Spiegelman, 1996) is a linear combination of the solid velocity \mathbf{U}_s and a vertical flow field driven by gravity. The weighting between the two flow fields depends on the permeability. If the permeability is low, fluids will follow solid velocity fields, whereas for high permeability, the flow will be primarily vertical. If vertical flow dominates, then the qualitative expectation is that carbonatite flow will lead the upwelling plume as is inferred from the ³He/⁴He signatures. Given the very small amount of carbonatite melt expected, however, a more quantitative estimate of the porosity/permeability is warranted to determine the magnitude of this effect.

Estimating the trajectories for carbonatite melts requires knowing the porosity produced by carbonatite melting for each trajectory. Because carbonatite melting is likely to occur over a narrow pressure range, we can use simple 1-D melting column theory to estimate this porosity.

Following Spiegelman and Elliott (1993) the relationship between the melt flux ϕw_l and the solid velocity W_s at the top of a 1-D adiabatically melting column is approximately:

$$\rho_l \phi w_l = \rho_s F_{max} W_s \quad (4)$$

where F_{max} is the degree of melting at the top of the column.

In the absence of viscous compaction effects (as is likely in the case of a rising plume), and under the assumption that buoyancy is the dominant driving force, the ascent velocities of the liquid and of the solid through a porous rock satisfy Darcy's law:

$$\phi w_l - \phi W_s = \frac{d^2 \phi^3}{C} \frac{\Delta \rho g}{\mu} \quad (5)$$

By combining Eqs. (4) and (5) we obtain:

$$\frac{W_s \rho_s F_{max}}{\rho_l} - \phi W_s = \frac{d^2 \phi^3}{C} \frac{\Delta \rho g}{\mu} \quad (6)$$

which provides an estimate of the porosity at the end of carbonatite melting as a function of solid upwelling rate, permeability and degree of melting. The use of F_{max} is justified by the fact that in a plume containing a very small amount of CO₂, which during ascent forms a small amount of carbonatite liquid, the maximum melt fraction is controlled by the available amount of CO₂ initially in the solid phases. Because the melting interval is small, F_{max} is reached relatively quickly.

Using Eq. (6), we calculate porosity as a function of grain diameter (Fig. 5a) for two different values of F_{max} , corresponding to carbonatite liquid contents of 870 and 1650 ppm, and for two different vertical solid velocities W_s of 1 and 0.1 m/yr. Using Eq. (5) we determine the separation velocity ($w_{sep} \equiv w_l - W_s$) as a function of grain diameter (Fig. 5b).

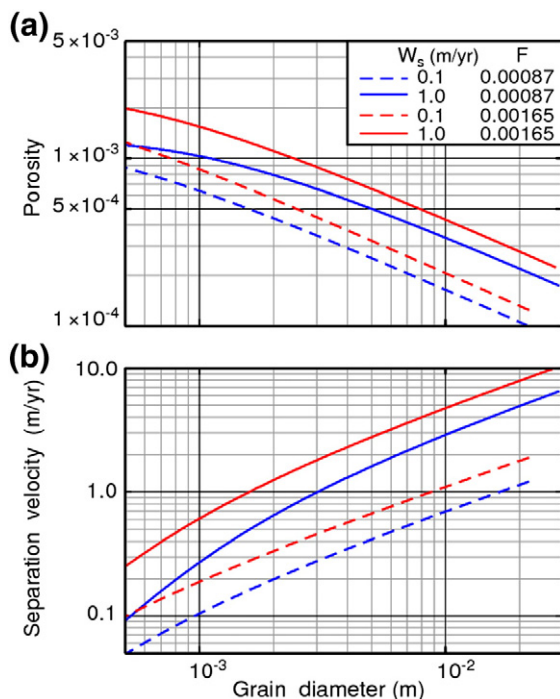


Fig. 5. (a) Porosity vs. grain diameter, calculated using Eq. (6), for a carbonatite liquid (see text). The values of degree of melting 0.00087 (blue) and 0.00165 (red) correspond to two estimates of the carbon content of the plume. The solid vertical velocities of 1.0 m/yr (solid lines) and 0.1 m/yr (dashed lines) correspond to values at the conduit center and periphery, respectively. (b) Separation velocity vs. grain diameter, calculated using Eq. (5) (see text). (For interpretation of the references to color in this figure legend, the reader is referred to the web version of this article.)

Some of the relationships shown in Fig. 5 may be surprising at first sight: For example, the porosity depends only relatively weakly on the maximum melt fraction, but more strongly on the grain diameter. The ascent velocity of the plume has a strong effect on the porosity, because it ultimately determines the production rate of carbonatite melt. In any case, the most important finding for the purpose of this paper is the high separation velocities, which range from tens of centimeters to several meters per year.

The highest separation velocities are obtained for the maximum grain diameter assumed, namely 30 mm. Earlier considerations of melt metasomatism (McKenzie, 1985) have usually estimated grain diameters on the order of 1 mm. But recently, Behn et al. (2009) have argued that, in the upper mantle, grain diameters of 10 to 30 mm are more likely, as a result of the competing processes of grain diminution by shear flow and grain growth. Whether this estimate will also hold for grain diameters within plumes remains to be seen. Shear, and therefore grain diminution, should be much greater than in normal asthenosphere, but grain growth should also be considerably faster due to higher temperatures and the presence of carbonatite melt. In any case, it is clear that this parameter, because of its strong effect on the migration velocities, contributes perhaps the greatest uncertainty to the quantitative results of our model.

6. Application to the Hawaiian plume

The model of the Hawaiian plume by Farnetani and Hofmann (2010) provides us with the three dimensional solid velocity field $\mathbf{U}_s = (U_s, V_s, W_s)$ used here to calculate both the porosity produced by carbonatite melting (Eq. (6)) and the trajectories of these liquids using Eqs. (2)–(3). An important feature of the simulated plume is that the upper part of the conduit is inclined in the direction of plate motion (Fig. 6). An inclined Hawaiian conduit is supported by global mantle flow models coupled to plate motions (Steinberger et al., 2004), by seismic tomography (Wolfe et al., 2009), and by a thin transition zone SE of the island of Hawaii (Schmerr et al., 2010). Note, however, the apparently contrary interpretation by Cao et al. (2011). Fig. 6a shows that the trajectories of the solid plume matrix are inclined in the direction of the overlying plate motion, whereas the counterflow is restricted to the extreme leading edge of the plume. Fig. 6 also indicates the melting zone for anhydrous peridotite (in yellow), and the onset of melting for carbonated peridotite (blue line in Fig. 6b and c), which is calculated using: $T_{solidus} = 1.475 P^2 + 44.38 P + 863.4$, where P is pressure in GPa. This formula is a parameterization provided by Dasgupta (2007, pers. comm.), extrapolated from experimental data below 10 GPa (Dasgupta and Hirschmann, 2006). Fig. 6b and c shows trajectories of carbonatite liquid for a grain size of $d = 1$ mm and for two different carbonate contents corresponding to $F_{max} = 0.00087$ and $F_{max} = 0.00165$. Since the solid velocity W_s at the carbonatite solidus ranges from about 1 m/yr in the center of the plume conduit to less than 0.1 m/yr close to the margins, the corresponding separation velocities of the carbonatite liquid range from 0.6 to 0.1 m/yr. Choosing a larger grain size would lead to even greater separation velocities (Fig. 5b) and therefore more vertical fluid trajectories. A common feature of all fluid trajectories is that the carbonatite liquid initially located in the plume center will move toward the leading edge of the plume. In contrast, carbonatite liquids initially located in the periphery on the trailing side of the plume stem will move toward the center. Thus, the more distant portions of the trailing side of the plume are invaded by small amounts of asthenosphere-derived carbonatite liquids.

In Fig. 6b and c the direction of carbonatite movement at each point depends on both the solid velocity field \mathbf{U}_s and a vertical component driven by gravity and permeability. In the center and on the left-hand side of the plume, the carbonatite ascends through progressively slower-moving solid material. Therefore the liquid trajectories become increasingly more vertical, in effect traversing from the

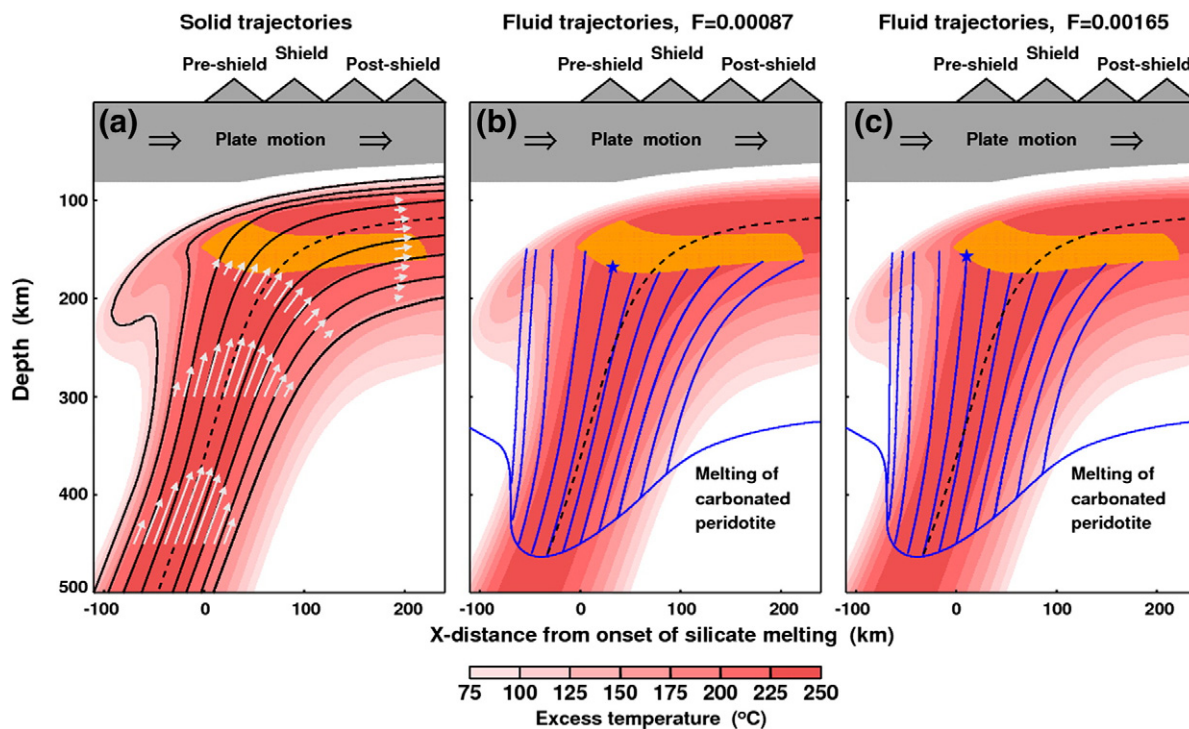


Fig. 6. Hawaiian plume model from Farnetani and Hofmann (2010). (a) Trajectories for the solid matrix (black lines), the central trajectory is dashed. Schematic solid velocity field (white arrows) and silicate melting zone (yellow field). (b) Trajectories for carbonatite fluids, calculated for carbon content $F = 0.00087$ and grain size $d = 0.001$ m (see text). The fluid central trajectory is marked by a star, for comparison the solid central trajectory is dashed. Trajectories start at the solidus of carbonate melting (thick blue line). (c) as (b), but for $F = 0.00165$. The overall effect is that the carbonatite liquid moves from the plume center toward the leading edge, and from the trailing underbelly toward the plume interior. Any helium carried by this carbonatite liquid will be displaced in the same manner. (For interpretation of the references to color in this figure legend, the reader is referred to the web version of this article.)

plume center toward its leading edge. On the right-hand side of the plume center, the opposite happens: The carbonatite liquid trajectories ascend through progressively faster moving plume material, and therefore the trajectories are deflected toward the horizontal, but they nevertheless move closer toward the center of the plume. Comparison of Fig. 6b and c shows that this ‘fanning effect’ at the underside of the plume is more pronounced when the overall separation velocity is low.

What happens to the carbonatite liquid once they reach shallow depths? As shown by Hirschmann (2010), the carbonatite is converted (by a continuous but probably rapid process) to silicate melt in the upper asthenosphere. Because of this, carbonatites are rare in OIB settings, and none has been found on Hawaiian volcanoes. The helium initially carried by the carbonatite is therefore ultimately erupted with the silicate melt (generally after substantial losses due CO_2 degassing of the silicate melt). Our approach of approximating these complex processes by two distinct stages, one involving pure carbonatite melt in the deeper part of the column, and one involving the formation and ultimate eruption of a silicate liquid, is thus a simplification, but it should nevertheless capture the essential features of the overall process.

In spite of the model limitations we can now ask: How does the ascending carbonate liquid affect the isotopic composition of the helium in the erupted lavas? For simplicity, we assume that (1) helium is quantitatively partitioned into the carbonate liquid, and (2) prior to carbonate melting the $^3\text{He}/^4\text{He}$ ratio decreases systematically from the center of the plume stem toward its margin. Since the distribution of $^3\text{He}/^4\text{He}$ ratios in the plume conduit is unknown, we tested two end-member models (Fig. 7). These profiles are calculated using the simulations by Farnetani and Hofmann (2009) of a plume conduit forming from a thermal boundary layer. In the first model (blue line in Fig. 7), R/R_a decreases as an error function across a thermal boundary layer of 100 km thickness. This corresponds

approximately to a plume source region with a diffusion profile of helium entering from a reservoir maintained at a uniform value of $R/R_a = 40$ (the maximum found in Loihi lavas), into an infinite medium with an initial $R/R_a = 8$ (the ambient MORB value). In the second model (dashed line in Fig. 7), R/R_a decreases linearly across the boundary layer. This corresponds to the case of a steady-state diffusion profile through a 100 km-thick layer in which both boundaries are maintained at constant R/R_a .

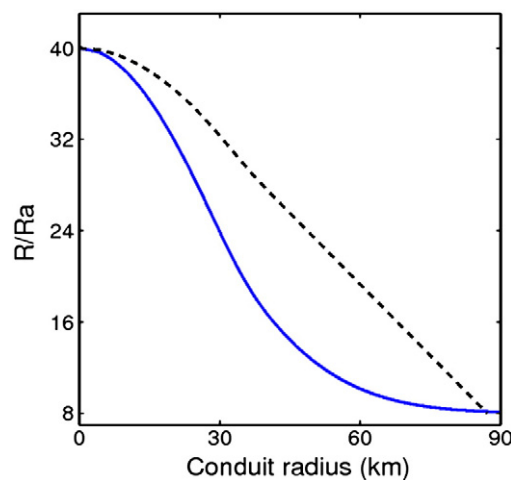


Fig. 7. R/R_a profiles vs. radial distance across the plume conduit at 450 km depth. The blue line corresponds to the case where R/R_a decreases as an error function across the thermal boundary layer at the base of the mantle. The dashed black line represents the corresponding case where R/R_a decreases linearly. These profiles serve as starting configurations for Figs. 8 and 9. (For interpretation of the references to color in this figure legend, the reader is referred to the web version of this article.)

Figures 8 and 9 show maps of R/Ra at the base of the silicate melting region and in the volcanoes for the two initial helium distributions of Fig. 7. Figs. 8a and 9a show map views of R/Ra in the absence of fluid ('solid trajectories'); panels b and c show the corresponding R/Ra distributions for the estimated lower and higher carbonate contents, $F_{max}=0.00087$ and $F_{max}=0.00165$. In the carbonate-present cases, the $^3\text{He}/^4\text{He}$ maximum is displaced from the silicate melting maximum by distances ranging from about 40 to 80 km. The greatest displacement is attained by the highest carbonate content (and the highest separation velocities). In addition, the rapidly ascending carbonatite liquid 'sharpens' the extent of high- $^3\text{He}/^4\text{He}$ relative to the carbonate-absent case.

Using these maps, we calculate the evolution of R/Ra during a volcano lifetime (Figs. 8 and 9, panels d, e, and f). We assume that a moving volcano is fed by magmas within a magma capture zone (MCZ) of 25 km radius. These magmas are assumed to ascend rapidly through subvertical channels into crustal magma chambers, from where they erupt. The calculated R/Ra ratio is shown for a central ($Y_{MCZ}=0$ km), an off-axis ($Y_{MCZ}=30$ km) and a peripheral ($Y_{MCZ}=50$ km) volcano. If helium is carried by the solid (Figs. 8d, 9d), pre-shield stage lavas are expected to have lower R/Ra values than during the shield stage, since the maximum R/Ra occurs at a distance of ~ 80 km from the onset of melting. In contrast, if helium is carried by the carbonatite fluids (panels e and f), pre-shield stage lavas have the highest R/Ra values, whereas shield and post-shield stages show progressively decreasing R/Ra, in agreement with observations at Hawaiian volcanoes (Figs. 2 and 3). We also predict that a central volcano has higher R/Ra than an off-axis or a peripheral volcano. In the framework of an axis-symmetric R/Ra distribution in the plume conduit, as assumed here,

this geographical difference could explain the higher R/Ra observed for the Loa-trend volcanoes, with respect to the more peripheral Kea-trend volcanoes, characterized by lower R/Ra. Although Figs. 8 and 9 differ in detail, their overall similarity suggests that the results are not very sensitive to the specific initial assumptions about the helium distribution in the conduit as long as the maximum R/Ra is in its center.

7. High R/Ra in the South Arch

The pronounced asymmetry of the Hawaiian distribution of helium shown in Fig. 2 extends to basalts from the North Arch (R/Ra < 10) and the South Arch (R/Ra up to 21; Hanyu et al., 2005), much farther than the extent of shield-building volcanism. Figs. 8 and 9 show that elevated $^3\text{He}/^4\text{He}$ ratios modeled here do extend beyond the onset of silicate melting by about 50 to 80 km. However, they do not reach nearly as far as the South Arch lavas, which are located about 200 km to the south of Loihi. This volcanic field erupted near the crest of the flexure zone surrounding the Hawaiian Islands; it consists of a few flows of alkalic basalts several meters thick and covers an area of about 35 by 50 km (Lipman et al., 1989). Their isotopic and elemental chemistry (e.g. $^{87}\text{Sr}/^{86}\text{Sr} \sim 0.7032$; Sims et al., 1995) clearly points to their derivation from the Hawaiian plume rather than a MORB-type source. Thus, although the South Arch lavas do not represent an early phase of Hawaiian shield volcanism, they appear to be derived from small amounts of low-viscosity, partially molten plume material that has spread well beyond the region where partial silicate melting occurs as modeled here. This discrepancy may be the result of our simplifying assumption that viscosity depends on temperature only. If the presence of partial melt causes an additional

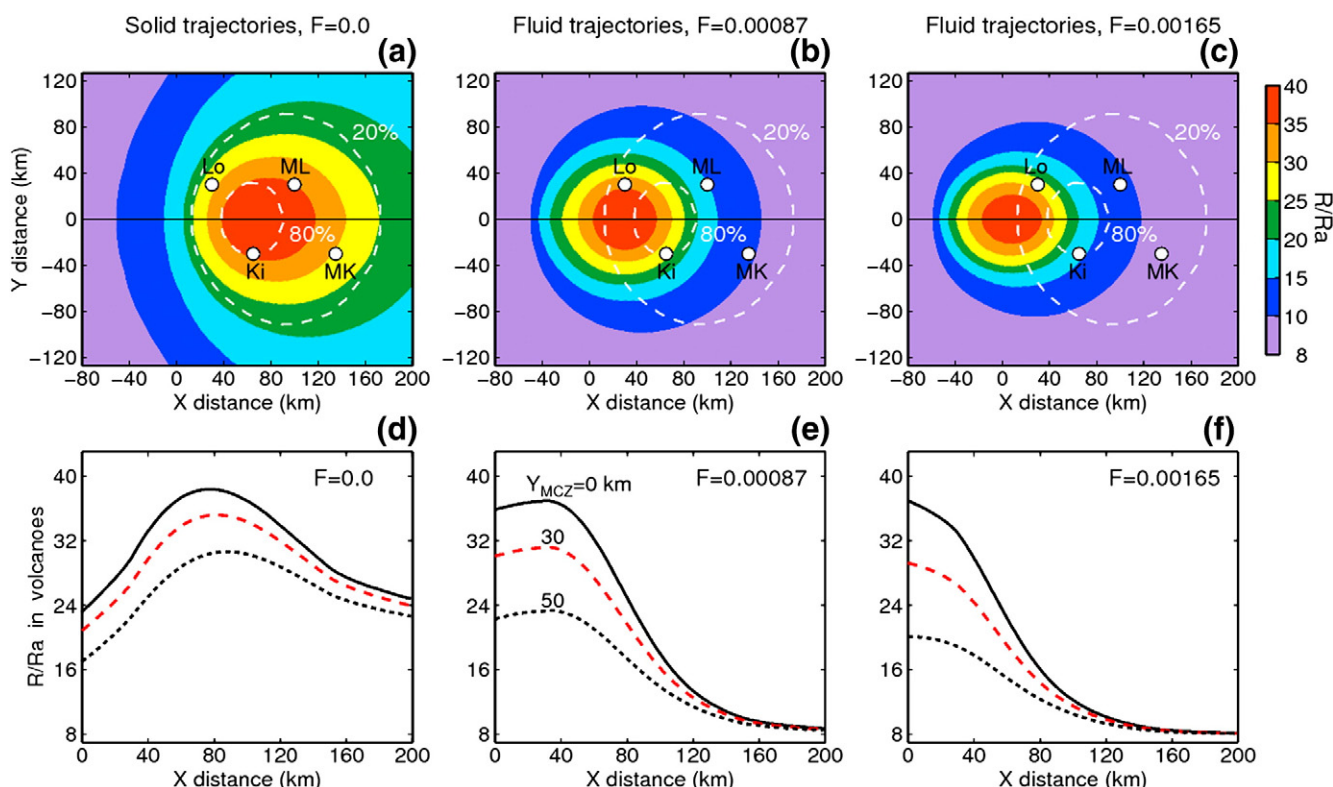


Fig. 8. Top: Maps of R/Ra calculated at the base of the silicate melting region, for the R/Ra radial profile given in Fig. 7 by the blue line. The X-distance is relative to the onset of silicate melting. White dashed lines delimit the zones where the silicate melt flux is 20% and 80% of the maximum value. A schematic location of some Hawaiian volcanoes is provided. (a) Map of R/Ra if helium is entirely carried by the solid ($F=0$). (b) Map of R/Ra if helium is carried by carbonatite fluids at $F=0.00087$. (c) Map of R/Ra if helium is carried by carbonatite fluids at $F=0.00165$. The maps illustrate the offset of the high R/Ra toward the leading edge of the plume relative to the distribution in a fluid-free plume. Bottom: Evolution of R/Ra in an individual volcano as a function of distance from the onset of silicate melting. Y_{MCZ} indicates the Y coordinate of the magma capture zone (MCZ) feeding the volcano: for a central volcano $Y_{MCZ}=0$ km (black solid line), for an off-axis volcano $Y_{MCZ}=30$ km (red dashed line), for a peripheral volcano $Y_{MCZ}=50$ km (black dashed line). (d), (e) and (f) correspond to the cases shown in (a), (b) and (c), respectively. (For interpretation of the references to color in this figure legend, the reader is referred to the web version of this article.)

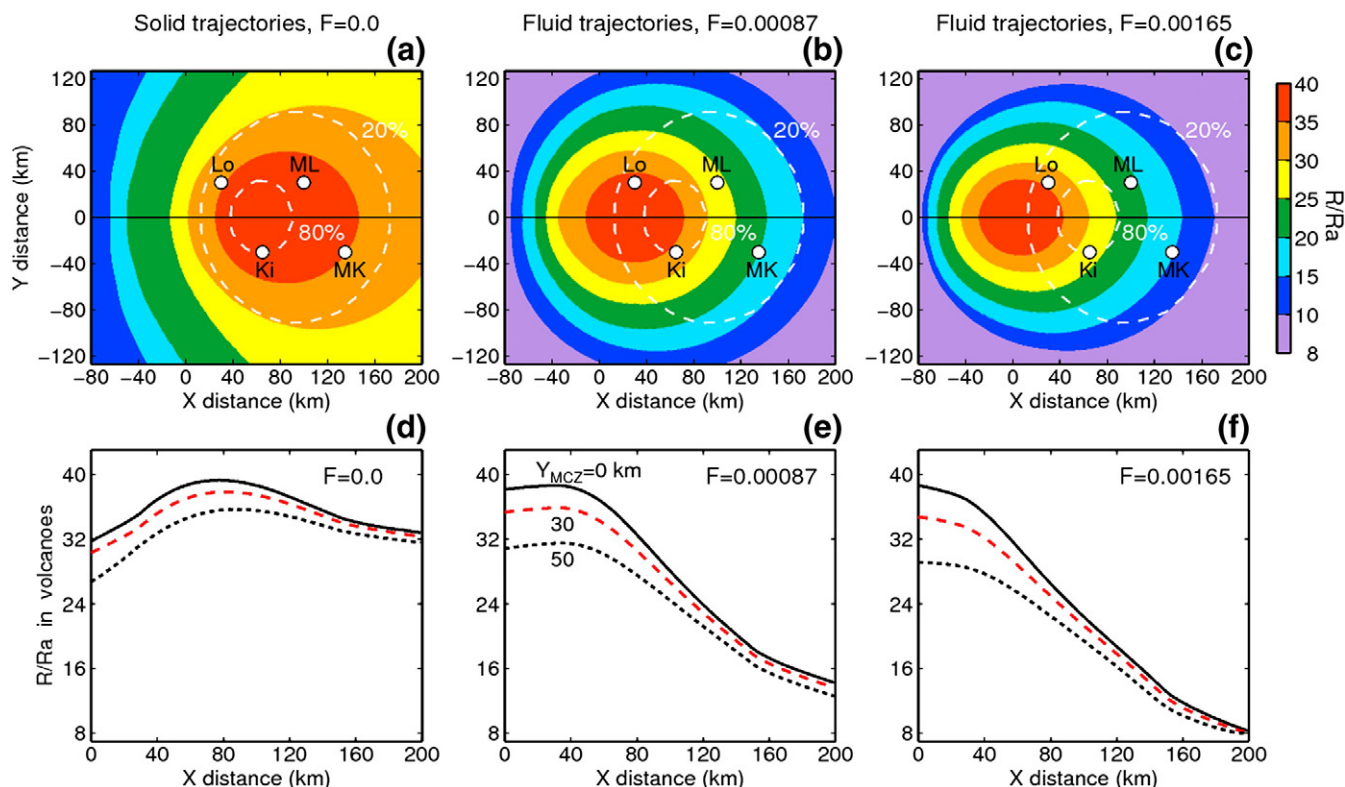


Fig. 9. Same as Fig. 8, but for the R/Ra radial profile given in Fig. 7 by the black dashed line.

lowering of viscosity, three-dimensional asthenospheric spreading of plume material may increase in all directions, including the direction ahead of the plume. Consequently, small amounts of Loihi-type silicate melts might be found farther ahead of the plume than has been modeled here.

8. Concluding remarks

We have compiled published evidence for a strong asymmetry in the distribution of ³He/⁴He ratios in Hawaiian basalts. Lavas erupted ahead of the main shield phases of volcanism have consistently higher R/Ra values than all known post-shield and rejuvenated lavas (and mantle xenoliths carried by these lavas), all of which have low, MORB-like R/Ra values. Three volcanoes for which the temporal evolution is well documented all show consistently declining R/Ra values during the shield phase.

Previous attempts to explain this invoked hydrous or carbonatitic metasomatic fluids moving in a dominantly lateral direction. Here we have modeled carbonatitic fluids rising predominantly vertically in a tilted plume conduit. The overall horizontal displacement of carbonatite and helium from the core of the conduit reaches distances of up to about 80 km in the upstream direction. This can explain the R/Ra maximum at the pre-shield stage (Loihi), the subsequent decline during the main shield-stage (Mauna Loa, Kilauea), and the low, MORB-type R/Ra in all post-shield volcanism. Our models have not addressed the question of decoupling of helium from other isotopic tracers, partly because the observations regarding decoupling are ambiguous and controversial at present, and partly because this would require greatly more elaborate fluid–solid simulations than would appear justified at this stage.

Our model can be tested by future observations both on the Hawaiian and on other oceanic mantle plumes where there is evidence for significant tilting of the conduit. Future seismological observations to determine the width and the tilt of the conduit will be critical. In addition we need further experimental progress on the onset of carbonatite

melting in the mantle and on the partition coefficients of helium and other trace elements in the carbonatite liquids. Ultimately, understanding the displacement behavior may help to resolve long-standing questions about the deep origin of plumes and the helium distribution in the mantle.

Acknowledgements

We thank Raj Dasgupta and Marc Hirschmann for in-depth advice on carbonatite melting in the mantle; Mark Kurz for kindly providing his compilation of dated Mauna Loa data; Jacqueline Dixon and Sujoy Mukhopadhyay for discussions. We also thank two anonymous reviewers for constructive reviews, and Yanick Ricard for his editorial handling. LDEO Contribution No. 7499; IPGP Contribution No. 3223.

References

Allègre, C.J., Moreira, M., 2004. Rare gas systematics and the origin of oceanic islands: the key role of entrainment at the 670 km boundary layer. *Earth Planet. Sci. Lett.* 228, 85–92.
 Allègre, C.J., Staudacher, T., Sarda, P., Kurz, M., 1983. Constraints on evolution of Earth's 640 mantle from rare gas systematics. *Nature* 303, 762–766.
 Althaus, T., Niedermann, S., Erzinger, J., 2003. Noble gases in olivine phenocrysts from drill core samples of the Hawaii Scientific Drilling Project (HSDP) pilot and main holes (Mauna Loa and Mauna Kea, Hawaii). *Geochem. Geophys. Geosyst.* 4. doi:10.1029/2001GC000275.
 Behn, M.D., Hirth, G., Elsenbeck II, J.R., 2009. Implications of grain size evolution on the seismic structure of the oceanic upper mantle. *Earth Planet. Sci. Lett.* 282, 178–189.
 Blichert-Toft, J., Albarède, F., 2009. Mixing and isotopic heterogeneities in the Mauna Kea plume conduit. *Earth Planet. Sci. Lett.* 282, 190–200.
 Boyet, M., Carlson, R.W., 2005. ¹⁴²Nd evidence for early (>4.53 Ga) global differentiation of the silicate Earth. *Science* 309, 576–581.
 Brandon, A.D., Graham, D.W., Waight, T., Gautason, B., 2007. ¹⁸⁶Os and ¹⁸⁷Os enrichments and high-³He/⁴He sources in the Earth's mantle: evidence from Icelandic picrites. *Geochim. Cosmochim. Acta* 71, 4570–4591.
 Breddam, K., Kurz, M.D., Storey, M., 2000. Mapping out the conduit of the Iceland mantle plume with helium isotopes. *Earth Planet. Sci. Lett.* 176, 45–55.
 Burnard, P., Toplis, M.J., Medynski, S., 2010. Low solubility of He and Ar in carbonatitic liquids: implications for decoupling noble gas and lithophile isotope systems. *Geochim. Cosmochim. Acta* 74, 1672–1683.

- Cao, Q., van der Hilst, R.D., de Hoop, M.V., Shim, S.-H., 2011. Seismic imaging of transition zone discontinuities suggests hot mantle west of Hawaii. *Science* 332, 1068–1071.
- Cartigny, P., Pineau, F., Aubaud, C., Javoy, M., 2008. Towards a consistent mantle carbon flux estimate: Insights from volatile systematics (H_2O/Ce , δD , CO_2/Nb) in the North Atlantic mantle (14°N and 34°N). *Earth Planet. Sci. Lett.* 265, 672–685.
- Class, C., Goldstein, S.L., 2005. Evolution of helium isotopes in the Earth's mantle. *Nature* 436, 1107–1112.
- Condomines, M., Grnvol, K., Hooker, P.J., Muehlenbachs, K., O'Nions, R.K., Oskarsson, N., Oxburgh, E.R., 1983. Helium, oxygen, strontium and neodymium relationships in Icelandic volcanics. *Earth Planet. Sci. Lett.* 66, 125–136.
- Connolly, J.A.D., Schmidt, M.W., Solferino, G., Bagdassarov, N., 2009. Permeability of ashenospheric mantle and melt extraction rates at mid-ocean ridges. *Nature* 462, 209–212.
- Courtillot, V.E., Davaille, A., Besse, J., Stock, J., 2003. Three distinct types of hotspots in the Earth's mantle. *Earth Planet. Sci. Lett.* 205, 295–308.
- Craig, H., Poreda, R.J., 1986. Cosmogenic He-3 in terrestrial rocks – the Summit Lavas of Maui. *Proc. Natl. Acad. Sci. U. S. A.* 83, 1970–1974.
- Dasgupta, R., Hirschmann, M.M., 2006. Melting in the Earth's deep upper mantle caused by carbon dioxide. *Nature* 440, 659–662.
- Dasgupta, R., Hirschmann, M.M., Withers, A.C., 2004. Deep global cycling of carbon constrained by the solidus of anhydrous, carbonated eclogite under upper mantle conditions. *Earth Planet. Sci. Lett.* 227, 73–85.
- Dasgupta, R., Hirschmann, M.M., McDonough, W.F., Spiegelman, M., Withers, A.C., 2009. Trace element partitioning between garnet lherzolite and carbonatite at 6.6 and 8.6 GPa with applications to the geochemistry of the mantle and of mantle-derived melts. *Chem. Geol.* 262, 57–77.
- DePaolo, D.J., Bryce, J.G., Dodson, A., Shuster, D.L., Kennedy, B.M., 2001. Isotopic evolution of Mauna Loa and the chemical structure of the Hawaiian plume. *Geochem. Geophys. Geosyst.* 2. doi:10.1029/2000GC000139.
- Dixon, E.T., 2003. Interpretation of helium and neon isotopic heterogeneity in Icelandic basalts. *Earth Planet. Sci. Lett.* 206, 83–99.
- Dixon, J.E., Clague, D.A., 2001. Volatiles in basaltic glasses from Loihi Seamount, Hawaii: evidence for a relatively dry plume component. *J. Petrol.* 42, 627–654.
- Dixon, E.T., Honda, M., McDougall, I., Campbell, I.H., Sigurdsson, I., 2000. Preservation of near-solar neon isotopic ratios in Icelandic basalts. *Earth Planet. Sci. Lett.* 180, 309–324.
- Dixon, J., Clague, D.A., Cousens, B., Monsalve, M.L., Uhl, J., 2008. Carbonatite and silicate melt metasomatism of the mantle surrounding the Hawaiian plume: evidence from volatiles, trace elements, and radiogenic isotopes in rejuvenated-stage lavas from Niihau, Hawaii. *Geochem. Geophys. Geosyst.* 9. doi:10.1029/2008GC002076.
- Eiler, J.M., Farley, K.A., Stolper, E.M., 1998. Correlated helium and lead isotope variations in Hawaiian lavas. *Geochim. Cosmochim. Acta* 62, 1977–1984.
- Eisele, J., Abouchami, W., Galer, S.J.G., Hofmann, A.W., 2003. The 320 ky Pb isotope evolution of the Mauna Kea lavas recorded in the HSDP-2 drill core. *Geochem. Geophys. Geosyst.* 4. doi:10.1029/2002GC000339.
- Farley, K.A., Natland, J.H., Craig, H., 1992. Binary mixing of enriched and undegassed (primitive?) mantle components (He, Sr, Nd, Pb) in Samoan lavas. *Earth Planet. Sci. Lett.* 111, 183–199.
- Farnetani, C.G., Hofmann, A.W., 2009. Dynamics and internal structure of a lower mantle plume conduit. *Earth Planet. Sci. Lett.* 282, 314–322.
- Farnetani, C.G., Hofmann, A.W., 2010. Dynamics and internal structure of the Hawaiian plume. *Earth Planet. Sci. Lett.* 295, 231–240.
- Garcia, M.O., Rubin, K.H., Norman, M.D., Rhodes, J.M., Graham, D.W., Muenow, D.W., Spencer, K., 1998. Petrology and geochronology of basalt breccia from the 1996 earthquake swarm of Loihi seamount, Hawaii – magmatic history of its 1996 eruption. *Bull. Volcanol.* 59, 577–592.
- Gerlach, T.M., Graeber, E.J., 1985. Volatile budget of Kilauea volcano. *Nature* 313, 273–277.
- Ghosh, S., Ohtani, E., Litasov, K., Suzuki, A., Sakamaki, T., 2007. Stability of carbonated magmas at the base of the Earth's upper mantle. *Geophys. Res. Lett.* 34, L22312 doi:10.1029/2007GL031349.
- Ghosh, S., Ohtani, E., Litasov, K.D., Terasaki, H., 2009. Solidus of carbonated peridotite from 10 to 20 GPa and origin of magnesioeclogite melt in the Earth's deep mantle. *Chem. Geol.* 262, 17–28.
- Gonnermann, H.M., Mukhopadhyay, S., 2009. Preserving noble gases in a convecting mantle. *Nature* 459, 560–563.
- Graham, D.W., 2002. Noble gas isotope geochemistry of mid-ocean ridge and ocean island basalts: characterization of mantle source reservoirs. In: Porcelli, D., et al. (Ed.), *Noble Gases Geochemistry and Cosmochemistry*: Mineral. Soc. Am., Washington, D.C., pp. 247–317.
- Graham, D.W., Johnson, K.T.M., Priebe, L.D., Lupton, J.E., 1999. Hotspot-ridge interaction along the Southeast Indian Ridge near Amsterdam and St. Paul islands: helium isotope evidence. *Earth Planet. Sci. Lett.* 167, 297–310.
- Hammouda, T., 2003. High-pressure melting of carbonated eclogite and experimental constraints on carbon recycling and storage in the mantle. *Earth Planet. Sci. Lett.* 214, 357–368.
- Hammouda, T., Laporte, D., 2000. Ultrafast mantle impregnation by carbonatite melts. *Geology* 28, 283–285.
- Hanyu, T., Clague, D.A., Kaneoka, I., Dunai, T.J., Davies, G.R., 2005. Noble gas systematics of submarine alkalic lavas near the Hawaiian hotspot. *Chem. Geol.* 214, 135–155.
- Hanyu, T., Johnson, K.T.M., Hirano, N., Ren, Z.-Y., 2007. Noble gas and geochronology study of the Hana Ridge, Haleakala volcano, Hawaii: implications to the temporal change of magma source and the structural evolution of the submarine ridge. *Chem. Geol.* 238, 1–18.
- Hanyu, T., Kimura, J.-I., Katakuse, M., Calvert, A.T., Sisson, T.W., Nakai, S.I., 2010. Source materials for inception stage Hawaiian magmas: Pb–He isotope variations for early Kilauea. *Geochem. Geophys. Geosyst.* 11 (Q0AC01). doi:10.1029/2009GC002760.
- Harpp, K.S., White, W.M., 2001. Tracing a mantle plume: isotopic and trace element variations of Galápagos seamounts. *Geochem. Geophys. Geosyst.* 2 Article number 2000GC000137.
- Heber, V.S., Brooker, R.A., Kelley, S.P., Wood, B.J., 2007. Crystal-melt partitioning of noble gases (helium, neon, argon, krypton, and xenon) for olivine and clinopyroxene. *Geochem. Cosmochim. Acta* 71, 1041–1061.
- Hilton, D.R., Thirlwall, M.F., Taylor, R.N., Murton, B.J., Nichols, A., 2000. Controls on magmatic degassing along the Reykjanes Ridge with implications for the helium paradox. *Earth Planet. Sci. Lett.* 183, 43–50.
- Hirschmann, M.M., 2010. Partial melt in the oceanic low velocity zone. *Phys. Earth Planet. Inter.* 179, 60–71.
- Honda, M., McDougall, I., Patterson, D.B., 1991. Possible solar noble-gas component in Hawaii basalts. *Nature* 349, 149–151.
- Honda, M., McDougall, I., Patterson, D.B., Doulgeris, A., Clague, D.A., 1993. Noble gases in submarine pillow basalt glasses from Loihi and Kilauea, Hawaii: a solar component in the Earth. *Geochem. Cosmochim. Acta* 57, 859–874.
- Hyagon, H., Ozima, M., Marty, B., Zashu, S., Sakai, H., 1992. Noble gases in submarine glasses from mid-ocean ridges and Loihi seamount: constraints on the early history of the Earth. *Geochem. Cosmochim. Acta* 56, 1301–1316.
- Jackson, M.G., Hart, S.R., Saal, A.E., Shimizu, N.K., Kurz, M.D., Blusztajn, J.S., Skovgaard, A.C., 2008. Globally elevated titanium, tantalum, and niobium (TITAN) in ocean island basalts with high $^3He/^4He$. *Geochem. Geophys. Geosyst.* 9. doi:10.1029/2007GC001876.
- Kaneoka, I., Takaoka, N., Clague, D.A., 1983. Noble gas systematics for coexisting glass and olivine crystals in basalts and dunite xenoliths from Loihi Seamount. *Earth Planet. Sci. Lett.* 66, 427–437.
- Kent, A.J.R., Clague, D.A., Honda, M., Stolper, E.M., Hutcheon, I.D., Norman, M.D., 1999. Widespread assimilation of a seawater-derived component at Loihi Seamount, Hawaii. *Geochim. Cosmochim. Acta* 63, 2749–2761.
- Koster van Groos, A.F., Wyllie, P.J., 1973. Liquid immiscibility in join $NaAlSi_3O_8$ – $CaAl_2Si_2O_8$ – Na_2CO_3 – H_2O . *Am. J. Sci.* 273, 465–487.
- Kurz, M.D., 1986. In situ production of terrestrial cosmogenic helium and some applications to geochronology. *Geochim. Cosmochim. Acta* 50, 2855–2862.
- Kurz, M.D., Kammer, D.P., 1991. Isotopic evolution of Mauna Loa volcano. *Earth Planet. Sci. Lett.* 103, 257–269.
- Kurz, M.D., Jenkins, W.J., Hart, S.R., Clague, D., 1983. Helium isotopic variations in volcanic rocks from Loihi Seamount and the Island of Hawaii. *Earth Planet. Sci. Lett.* 66, 388–406.
- Kurz, M.D., Meyer, P.S., Sigurdsson, H., 1985. Helium isotopic systematics within the neovolcanic zones of Iceland. *Earth Planet. Sci. Lett.* 74, 291–305.
- Kurz, M.D., Garcia, M.O., Frey, F.A., O'Brien, P.A., 1987. Temporal helium isotopic variations within Hawaiian volcanoes; basalts from Mauna Loa and Haleakala. *Geochim. Cosmochim. Acta* 51, 2905–2914.
- Kurz, M.D., Kenna, T.C., Kammer, D.P., Rhodes, J.M., Garcia, M.O., 1995. Isotopic evolution of Mauna Loa Volcano: a view from the submarine Southwest Rift Zone. In: Rhodes, J.M., Lockwood, J.P. (Eds.), *Mauna Loa Revealed: Structure, Composition, History and Hazards*. Am. Geophys. Union, Washington, D.C., pp. 289–306.
- Kurz, M.D., Kenna, T.C., Lassiter, J.C., DePaolo, D.J., 1996. Helium isotopic evolution of Mauna Kea Volcano: first results from the 1-km drill core. *J. Geophys. Res.* 101, 11,781–11,791.
- Kurz, M.D., Curtice, J., Lott, D.E., Solow, A., 2004. Rapid helium isotopic variability in Mauna Kea shield lavas from the Hawaiian Scientific Drilling Project. *Geochem. Geophys. Geosyst.* 5. doi:10.1029/2002GC000439.
- Kyser, T.K., Rison, W., 1982. Systematics of rare gas isotopes in basic lavas and ultramafic xenoliths. *J. Geophys. Res.* 87, 5611–5630.
- Lee, W.J., Wyllie, P.J., 1996. Liquid immiscibility in the join $NaAlSi_3O_8$ – $CaCO_3$ to 2 center dot 5 GPa and the origin of calcioeclogite magmas. *J. Petrol.* 37, 1125–1152.
- Licciardi, J.M., Kurz, M.D., Curtice, J.M., 2006. Cosmogenic 3He production rates from Holocene lava flows in Iceland. *Earth Planet. Sci. Lett.* 246, 251–264.
- Lipman, P.W., Clague, D.A., Moore, J.G., Holcomb, R.T., 1989. South Arch volcanic field – newly identified young lava flows on the sea floor south of the Hawaiian Ridge. *Geology* 17, 611–614.
- Macpherson, C.G., Hilton, D.R., Day, J.M.D., Lowry, D., K., G., 2005. High- $^3He/^4He$, depleted mantle and low- $\delta^{18}O$, recycled oceanic lithosphere in the source of central Iceland magmatism. *Earth Planet. Sci. Lett.* 233, 411–427.
- Marti, K., Craig, H., 1987. Cosmic-ray-produced neon and helium in the summit lavas of Maui. *Nature* 325, 335–337.
- Marty, B., Tolstikhin, I.N., 1998. CO_2 fluxes from mid-ocean ridges, arcs and plumes. *Chem. Geol.* 145, 233–248.
- Matsumoto, T., Orihashi, Y., Matsuda, J.-I., Yamamoto, K., 2008. Argon isotope ratio of the plume-source deduced from high-resolution stepwise crushing extraction. *Geochem. J.* 42, 39–49.
- McKenzie, D., 1985. The extraction of magma from the crust and mantle. *Earth Planet. Sci. Lett.* 74, 81–91.
- Mihalffy, P., Steinberger, B., Schmeling, H., 2008. The effect of the large-scale mantle flow field on the Iceland hotspot track. *Tectonophysics* 447, 5–18.
- Minarik, W.G., Watson, E.B., 1995. Interconnectivity of carbonate melt at low melt fraction. *Earth Planet. Sci. Lett.* 133, 423–437.
- Moreira, M., Breddam, K., Curtice, J., Kurz, M.D., 2001. Solar neon in the Icelandic mantle: new evidence for an undegassed lower mantle. *Earth Planet. Sci. Lett.* 185, 15–23.
- Mukhopadhyay, S., Lassiter, J.C., Farley, K.A., Bogue, S.W., 2003. Geochemistry of Kauai shield-stage lavas: implications for the chemical evolution of the Hawaiian plume. *Geochem. Geophys. Geosyst.* 4. doi:10.1029/2002GC000342.

- Murton, B.J., Taylor, R.N., Thirlwall, M.F., 2002. Plume–ridge interaction: a geochemical perspective from the Reykjanes Ridge. *J. Petrol.* 43, 1987–2012.
- Nicolaysen, K.P., Frey, F.A., Mahoney, J.J., Johnson, K.T.M., Graham, D.W., 2007. Influence of the Amsterdam/St. Paul hot spot along the Southeast Indian Ridge between 77 degrees and 88 degrees E: correlations of Sr, Nd, Pb, and He isotopic variations with ridge segmentation. *Geochem. Geophys. Geosyst.* 8. doi:10.1029/2006GC001540.
- Parman, S.W., Kurz, M.D., Hart, S.R., Grove, T.L., 2005. Helium solubility in olivine and implications for high $^3\text{He}/^4\text{He}$ in ocean island basalts. *Nature* 437, 1140–1143.
- Porcelli, D., Halliday, A.N., 2001. The core as a possible source of mantle helium. *Earth Planet. Sci. Lett.* 192, 45–56.
- Porcelli, D.R., Stone, J.O.H., O'Nions, R.K., 1987. Enhanced ratios and cosmogenic helium in ultramafic xenoliths. *Chem. Geol.* 64, 25–33.
- Poreda, R., Schilling, J.-G., Craig, H., 1986. Helium and hydrogen isotopes in ocean-ridge basalts north and south of Iceland. *Earth Planet. Sci. Lett.* 78, 1–17.
- Ren, Z.-Y., Hanyu, T., Miyazaki, T., Chang, Q., Kawabata, H., Takahashi, T., Hirahara, Y., Nichols, A.R.L., Tatsumi, Y., 2009. Geochemical differences of the Hawaiian shield lavas: implications for melting process in the heterogeneous Hawaiian plume. *J. Petrol.* 50, 1553–1573.
- Rison, W., Craig, H., 1983. Helium isotopes and mantle volatiles in Loihi Seamount and Hawaiian Island basalts and xenoliths. *Earth Planet. Sci. Lett.* 66, 407–426.
- Saal, A., Hauri, E., Langmuir, C.H., Perfit, M.R., 2002. Vapour undersaturation in primitive mid-ocean-ridge basalt and the volatile content of Earth's upper mantle. *Nature* 419, 451–455.
- Samuel, H., Farnetani, C.G., 2003. Thermochemical convection and helium concentrations in mantle plumes. *Earth Planet. Sci. Lett.* 207, 39–56.
- Sarda, P., Staudacher, T., Allègre, C.J., 1988. Neon isotopes in submarine basalts. *Earth Planet. Sci. Lett.* 91, 73–88.
- Scarsi, P., 2000. Fractional extraction of helium by crushing of olivine and clinopyroxene phenocrysts: effects on the $^3\text{He}/^4\text{He}$ measure ratio. *Geochim. Cosmochim. Acta* 64, 3751–3762.
- Schilling, J.-G., Kingsley, R.H., Fontignie, D., Poreda, R., Xue, S., 1999. Dispersion of the Jan Mayen and Iceland mantle plumes in the Arctic: a He–Pb–Nd–Sr isotope tracer study of basalts from the Kolbeinsey, Mohns, and Knipovich Ridges. *J. Geophys. Res.* 104, 50543–510569.
- Schmerr, N., Garnero, E., McNamara, A., 2010. Deep mantle plumes and convective upwelling beneath the Pacific Ocean. *Earth Planet. Sci. Lett.* 294, 143–151.
- Shen, Y., Solomon, S.C., Bjarnason, I.T., Nolet, G., Morgan, W.J., Allen, R.M., Vogfjord, K., Jakobsdottir, S., Stefansson, R., Julian, B.R., Foulger, G.R., 2002. Seismic evidence for a tilted mantle plume and north–south mantle flow beneath Iceland. *Earth Planet. Sci. Lett.* 197, 261–272.
- Sims, K.W.W., DePaolo, D.J., Murrell, M.T., Baldrige, W.S., Goldstein, S.J., Clague, D.A., 1995. Mechanisms of magma generation beneath Hawaii and mid-ocean ridges: uranium/thorium and samarium/neodymium isotopic evidence. *Science* 267, 508–512.
- Sobolev, A.V., Hofmann, A.W., Sobolev, S.V., Nikogosian, I.K., 2005. An olivine-free mantle source of Hawaiian shield basalts the source of Mauna Loa lavas. *Nature* 434, 590–597.
- Spiegelman, M., 1993a. Flow in deformable porous-media .1. Simple analysis. *J. Fluid Mech.* 247, 17–38. doi:10.1017/S0022112093000369.
- Spiegelman, M., 1993b. Flow in deformable porous-media .2. Numerical analysis—the relationship between shock-waves and solitary waves. *J. Fluid Mech.* 247, 39–63. doi:10.1017/S0022112093000370.
- Spiegelman, M., 1996. Geochemical consequences of melt transport in 2-D: the sensitivity of trace elements to mantle dynamics. *Earth Planet. Sci. Lett.* 139, 115–132.
- Spiegelman, M., Elliott, T., 1993. Consequences of melt transport for uranium series disequilibrium in young lavas. *Earth Planet. Sci. Lett.* 118, 1–20.
- Stagno, V., Frost, D.J., 2010. Carbon speciation in the asthenosphere: experimental measurements of the redox conditions at which carbonate-bearing melts coexist with graphite or diamond in peridotite assemblages. *Earth Planet. Sci. Lett.* 300, 72–84.
- Staudacher, T., Kurz, M.D., Allègre, C.J., 1986. New noble-gas data on glass samples from Loihi Seamount and Hualalai and on dunite samples from Loihi and Réunion Island. *Chem. Geol.* 56, 193–205.
- Steinberger, B., Sutherland, R., O'Connell, R.J., 2004. Prediction of Emperor-Hawaii seamount locations from a revised model of global plate motion and mantle flow. *Nature* 430, 167–173.
- Taylor, R.N., Thirlwall, M.F., Murton, B.J., Hilton, D.R., Gee, M.A.M., 1997. Isotopic constraints on the influence of the Icelandic plume. *Earth Planet. Sci. Lett.* 148, E1–E8.
- Tolstikhin, I.N., Hofmann, A.W., 2005. Early crust on top of the Earth's core. *Phys. Earth Planet. Inter.* 148, 109–130.
- Tolstikhin, I.N., Kramers, J.D., Hofmann, A.W., 2006. A chemical Earth model with whole mantle convection: the importance of a core–mantle boundary layer (D") and its early formation. *Chem. Geol.* 226, 79–99.
- Treiman, A.H., Schedl, A., 1983. Properties of carbonatite magma and processes in carbonatite magma chambers. *J. Geol.* 91, 437–447.
- Trull, T., Nadeau, S., Pineau, F., Polvé, M., Javoy, M., 1993. C–He systematics in hotspot xenoliths: implications for mantle carbon contents and carbon recycling. *Earth Planet. Sci. Lett.* 118, 43–64.
- Valbracht, P.J., Staudigel, H., Honda, M., McDougall, I., Davies, G.R., 1996. Isotopic tracing of volcanic source regions from Hawaii: decoupling of gaseous from lithophile magma components. *Earth Planet. Sci. Lett.* 144, 185–198.
- Valbracht, P.J., Staudacher, T., Malahoff, A., Allègre, C.J., 1997. Noble gas systematics of deep rift zone glasses from Loihi Seamount, Hawaii. *Earth Planet. Sci. Lett.* 150, 399–411.
- Vance, D., Stone, J.O.H., O'Nions, R.K., 1989. He, Sr and Nd isotopes in xenoliths from Hawaii and other oceanic islands. *Earth Planet. Sci. Lett.* 96, 147–160.
- Wark, D.A., Williams, C.A., Watson, E.B., Price, J.D., 2003. Reassessment of pore shapes in microstructurally equilibrated rocks, with implications for permeability of the upper mantle. *J. Geophys. Res.* 108. doi:10.1029/2001JB001575.
- Wolfe, C.J., Solomon, S.C., Laske, G., Collins, J.A., Detrick, R.S., Orcutt, J.A., Bercovici, D., Hauri, E.H., 2009. Mantle shear-wave velocity structure beneath the hawaiian hot spot. *Science* 326, 1388–1390.
- Yaxley, G.M., Brey, G.P., 2004. Phase relations of carbonate-bearing eclogite assemblages from 2.5 to 5.5 GPa: implications for petrogenesis of carbonatites. *Contrib. Mineral. Petrol.* 146, 606–619.